AFRL-VA-WP-TP-2007-304

OUTPUT FEEDBACK CONTROL AND SENSOR PLACEMENT FOR A HYPERSONIC VEHICLE MODEL (PREPRINT)

Pete Jankovsky, David O. Sigthorsson, Andrea Serrani, Stephen Yurkovich, Michael A. Bolender, and David B. Doman

DECEMBER 2006

STINFO COPY

AIR VEHICLES DIRECTORATE
AIR FORCE MATERIEL COMMAND
AIR FORCE RESEARCH LABORATORY
WRIGHT-PATTERSON AIR FORCE BASE, OH 45433-7542

NOTICE AND SIGNATURE PAGE

AFRL-VA-WP-TP-2007-304 HAS BEEN REVIEWED AND IS APPROVED FOR PUBLICATION IN ACCORDANCE WITH ASSIGNED DISTRIBUTION STATEMENT.

*//Signature//

MICHAEL A. BOLENDER
Aerospace Engineer
Air Force Research Laboratory
Air Vehicles Directorate

//Signature//

DEBORAH S. GRISMER
Chief, Control Design and Analysis Branch
Air Force Research Laboratory
Air Vehicles Directorate

//Signature//

JEFFREY C. TROMP
Senior Technical Advisor
Control Sciences Division
Air Vehicles Directorate

REPORT DOCUMENTATION PAGE

1. REPORT DATE *(DD-MM-YY)*	2. REPORT TYPE	3. DATES COVERED *(From - To)*
December 2006	Conference Paper Preprint	06/15/2006 – 12/31/2006

4. TITLE AND SUBTITLE

OUTPUT FEEDBACK CONTROL AND SENSOR PLACEMENT FOR A HYPERSONIC VEHICLE MODEL (PREPRINT)

5a. CONTRACT NUMBER
F33615-01-2-3154

5b. GRANT NUMBER

5c. PROGRAM ELEMENT NUMBER
N/A

6. AUTHOR(S)

Pete Jankovsky, David O. Sigthorsson, Andrea Serrani, and Stephen Yurkovich (The Ohio State University)
Michael A. Bolender and David B. Doman (AFRL/VACA)

5d. PROJECT NUMBER
N/A

5e. TASK NUMBER
N/A

5f. WORK UNIT NUMBER
N/A

7. PERFORMING ORGANIZATION NAME(S) AND ADDRESS(ES)

The Ohio State University
Collaborative Center for Control Science
Department of Electrical and Computer
Engineering, 2015 Neil Ave.
Columbus, OH 43210

Control Design and Analysis Branch (AFRL/VACA)
Control Sciences Division
Air Vehicles Directorate
Air Force Materiel Command
Air Force Research Laboratory
Wright-Patterson Air Force Base, OH 45433-7542

8. PERFORMING ORGANIZATION REPORT NUMBER

9. SPONSORING/MONITORING AGENCY NAME(S) AND ADDRESS(ES)

Air Vehicles Directorate
Air Force Research Laboratory
Air Force Materiel Command
Wright-Patterson Air Force Base, OH 45433-7542

10. SPONSORING/MONITORING AGENCY ACRONYM(S)
AFRL-VA-WP

11. SPONSORING/MONITORING AGENCY REPORT NUMBER(S)
AFRL-VA-WP-TP-2007-304

12. DISTRIBUTION/AVAILABILITY STATEMENT
Approved for public release; distribution unlimited.

13. SUPPLEMENTARY NOTES

14. ABSTRACT

This paper addresses issues related to output feedback control, including sensor placement, for a model of an air-breathing hypersonic vehicle. The model presents a number of control challenges, in particular because of strong couplings between the propulsive and aerodynamic forces. Because of the vehicle's low weight, slenderness, and length, the vehicle's flexibility has a large impact on stability and control of the vehicle. Two output feedback control methods are developed. One applies reconstruction of the flexible body system states, toward applications of state feedback control. The other uses a robust design that does not rely on an observer to ensure stabilization and performance throughout a given flight envelope. A rate gyroscope and an accelerometer have been modeled, incorporating the flexible effects, and strategies for sensor placement have been developed for the hypersonic vehicle model to enhance observability or to preserve certain system structures that are favorable for robust control design. Simulation results are provided to demonstrate the sensor placement strategies and output feedback control performances.

15. SUBJECT TERMS
Flight Control, Hypersonic Vehicles

16. SECURITY CLASSIFICATION OF:

a. REPORT	b. ABSTRACT	c. THIS PAGE	17. LIMITATION OF ABSTRACT:	18. NUMBER OF PAGES	19a. NAME OF RESPONSIBLE PERSON (Monitor)
Unclassified	Unclassified	Unclassified	SAR	28	Michael A. Bolender

19b. TELEPHONE NUMBER *(Include Area Code)*
N/A

Output Feedback Control and Sensor Placement for a Hypersonic Vehicle Model

Pete Jankovsky [*]

David O. Sigthorsson [*]

Andrea Serrani [†]

Stephen Yurkovich [‡]

Collaborative Center for Control Science,

The Ohio State University, Columbus, OH, 43210

Michael A. Bolender [§]

David B. Doman [¶]

Air Force Research Laboratory,

Wright-Patterson Air Force Base, Dayton, OH, 45433

This paper addresses issues related to output feedback control, including sensor placement, for a model of an air-breathing hypersonic vehicle. The model presents a number of control challenges, in particular because of strong couplings between the propulsive and aerodynamic forces. Because of the vehicle's low weight, slenderness, and length, the vehicle's flexibility has a large impact on stability and control of the vehicle. Two output feedback control methods are developed. One applies reconstruction of the flexible body system states, toward applications of state feedback control. The other uses a robust design that does not rely on an observer to ensure stabilization and performance throughout a given flight envelope. A rate gyroscope and an accelerometer have been modeled, incorporating the flexible effects, and strategies for sensor placement have been developed for the hypersonic vehicle model to enhance observability or to preserve certain system structures that are favorable for robust control design. Simulation results are provided to demonstrate the sensor placement strategies and output feedback control performances.

I. Introduction

Hypersonic air-breathing vehicles offer a promising technology for cost efficient and time reduced flights in both commercial and military applications. Quick response and space access meet the Air Force's need for global strike capabilities while providing significant advantages over expendable rockets. Recent success in NASA's X-43A's hypersonic vehicle affirms the scramjet engine technology for these applications.

Control designs are challenging because of unique characteristics of the hypersonic vehicle, particularly the strong coupling between propulsive and aerodynamic forces. The engine thrust affects the pitching moment due to the underslung location of the scramjet engine. The length, slender geometry, and relative light weight of the vehicle cause the vibrational modes to significantly affect the aerodynamic forces.[1,2] In addition, the model has critically stable internal dynamics and is statically unstable. A variety of approaches have been utilized for the general control problem in this setting; for example, designing a nonlinear controller that neglects the flexibility effects,[3,4] or using various linear state feedback controllers .[5–7] Related work

---

[*]Graduate Research Assistant, Department of Electrical and Computer Engineering, 2015 Neil Ave., Columbus, OH.

[†]Assistant Professor, Department of Electrical and Computer Engineering, 2015 Neil Ave., Columbus, OH.

[‡]Professor, Department of Electrical and Computer Engineering, 2015 Neil Ave., Columbus, OH.

[§]Aerospace Engineer, AFRL/VACA, 2210 Eighth St. Suite 21, Dayton, OH, Senior Member AIAA.

[¶]Senior Aerospace Engineer, AFRL/VACA, 2210 Eighth St. Suite 21, Dayton, OH, Assoc. Fellow AIAA.
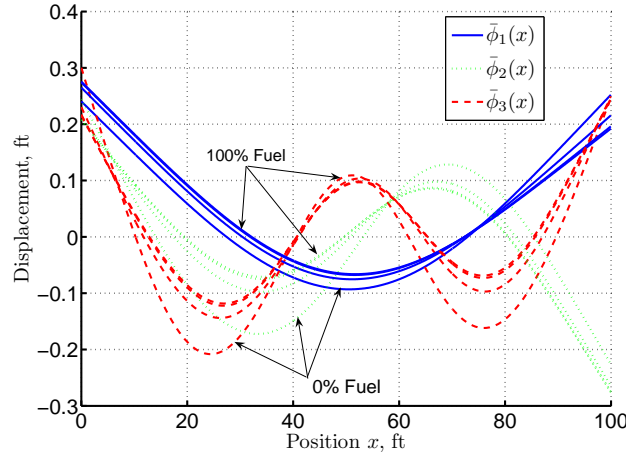
Figure 1. Geometry of the hypersonic vehicle model from Bolender and Doman.[1]

in the field considers longitudinal control through linearized models and control designs,[2,8] guidance,[9] and nonlinear methods,[10,11] many with dependence on access to full state information.

This paper utilizes linear control design by considering two output feedback control methods. In the first approach, partial state information is provided through the outputs and used to reconstruct full state information, which is then used with a state-feedback controller. The placement of the sensors strongly affects the system's observability, so sensor placement strategies are developed to increase observability or to preserve certain pole-zero structures that are favorable for robust control design. Our results for the hypersonic vehicle follow traditional sensor placement work for flight vehicles based on observability. In particular, Van der Velde and Carignan's free-free flexible beam model[12] closely agrees with our sensor placement results for the observer design. We also follow Al-Shehabi and Newman's[13] sensor placement strategies and optimization methods.

In the second approach, a robust output feedback strategy that does not rely on state observation is developed to overcome the limitations posed by linear observer-based controller. The methodology employs pre-compensation of the unstable zero-dynamics, dynamic extension, and a robust servomechanism design based on time-scale separation methods. The resulting controller, paired with a judicious placement of the sensor, is shown to yield superior tracking performance and improved robustness versus observer-based design for a large envelope of operating conditions.

The paper is organized as follows: Section II describes the hypersonic vehicle model and sensor modeling. In Section III the observer based output feedback controller is developed along with relevant sensor placement strategies. Section IV discusses the development of the robust output feedback design, including appropriate sensor placement. Simulation results are provided in Section V, and conclusions are given in Section VI.

II.   Hypersonic Vehicle Model

The hypersonic vehicle model considered in this paper is the assumed-modes version[14] of the model originally developed by Bolender and Doman.[1,15] In the cited references, the stability-axis equations of motion for the longitudinal dynamics of the hypersonic vehicle are derived through Lagrange's equations as

$$
\begin{aligned}
\dot{V}_t &= \frac{1}{m}(T\cos\alpha - D) - g\sin(\theta - \alpha) \\
\dot{\alpha} &= \frac{1}{mV_t}(-T\sin\alpha - L) + Q + \frac{g}{V_t}\cos\theta - \alpha \\
\dot{Q} &= \frac{M}{I_{yy}} \\
\dot{h} &= V_t\sin(\theta - \alpha) \\
\dot{\theta} &= Q \\
\ddot{\eta}_i &= -2\zeta_i\omega_i\dot{\eta}_i - \omega_i^2\eta_i + N_i \qquad i = 1,\ldots,n,
\end{aligned} \tag{1}
$$

American Institute of Aeronautics and Astronautics

Figure 2. Mass normalized flexible mode shapes as the fuel level is varied from empty to 50% -, 90% -, and 100% full.

where m is the vehicle mass, I_{yy} the moment of inertia, g the acceleration of gravity, and ζ_i and ω_i are the damping factor and the natural frequency of the i-th flexible mode, respectively. The aerodynamic forces enter (1) as lift L, drag D, thrust T, pitching moment M about the body y-axis, and the generalized elastic forces N_1, N_2, N_3. The control inputs $u_p = [\delta_e, \delta_c, \phi, A_d]^T$ appear implicitly in (1) through the aerodynamic forces, where δ_e is the elevator deflection angle, δ_c is the canard deflection angle, ϕ is the fuel to air ratio, and A_d is the diffuser area ratio. The plant model considered in this study comprises the eleven-dimensional state vector $x_p = [V_t, \alpha, Q, h, \theta, \eta_1, \dot{\eta}_1, \eta_2, \dot{\eta}_2, \eta_3, \dot{\eta}_3]^T$. The first five states are referred to as x_r, the rigid body states: vehicle velocity V_t, angle of attack α, pitch rate Q, altitude h, and pitch θ. The last six states are referred to as x_f, the flexible states, which consist of three vibrational displacements η_1, η_2, η_3 and their time derivatives. A sketch of the vehicle geometry is given in Figure 1.

The assumed modes version of the hypersonic vehicle model[14] considers the vehicle as a single flexible structure instead of clamped beams. This model removes the coupling between rigid body and flexible body dynamics, so that the flexible modes are orthogonal to the rigid body modes. The flexible effect interaction occurs only through the aerodynamic forces in (1). Only the first three modes are considered in this study. The vibrational model is defined as a traditional free-free beam[16] with mass normalized mode shapes $\bar{\phi}_i$ shown in Figure 2. The damping coefficient $\zeta = 0.02$ is constant, while the modal frequencies ω_i change with the operating conditions. The most noticeable effect influencing mode shapes and frequencies is the mass of the vehicle, which decreases as fuel is consumed. A fuel consumption model is not yet developed for the aircraft, so the fuel mass at trim condition is held constant throughout simulation. It is important to observe that while the shapes do not change much with fuel consumption, there are significant variations in node locations and modal frequencies. The four sets of curves in Figure 2 show the mode shape shifting behavior as fuel is consumed. A sample of change in modal frequency and node, anti-node and center of gravity locations for various fuel conditions is listed in Table 1.

Table 1. Selected first mode-shape frequencies and node/anti-node locations as vehicle mass changes.

	Available Fuel			
	0%	50%	90%	100%
m (slug)	9356.58	14786.39	19130.24	20216.21
ω_1 (rad/s)	22.77672	21.17379	20.3468	20.175
x_{cg} (ft)	53.1008	53.8218	54.1039	54.1555
$x_{\mathrm{node},1}$ (ft)	27.4	30.4	31.9	32.2
$x_{\mathrm{a-node},1}$ (ft)	50.5	51.1	51.6	51.7

American Institute of Aeronautics and Astronautics

A. Rate Gyroscope Sensor Model

The pitch rate of the aircraft can be measured by a rate gyroscope sensor; however, the rigid body pitch rate Q will be affected by the angular velocity contribution of the flexible beam.[12, 17] The measured pitch rate of the aircraft $Q_{f,j}$, as sensed by the jth rate gyroscope, is modeled as

$$Q_{f,j} = Q - \sum_{i=1}^{n} \frac{d\bar{\phi}_i(x_{\mathrm{rg},j})}{dx} \dot{\eta}_i, \tag{2}$$

where $x_{\mathrm{rg},j}$ is the location of each j rate gyroscope matched with spatial derivative for each ith mass normalized mode shape in Figure 2.

B. Accelerometer Sensor Model

Many aircraft designs use a self-aligning vane or flow direction sensor to measure the angle of attack; however, these traditional sensors will not suffice for hypersonic flight. Instead, we estimate the angle of attack trajectory from measurements of normal acceleration.[17] The body axis normal acceleration at the center of gravity, unaffected by the flexible states, is denoted n_{z}. Because our aircraft model only considers longitudinal motion, we neglect rolling motion and normalize the acceleration to g-units. This is implemented in simulation with the stability axis equation:

$$\frac{n_{\mathrm{z}}}{g} = \frac{-D \sin \alpha}{mg} - \frac{L \cos \alpha}{mg} + \cos \theta. \tag{3}$$

Away from the center of gravity at a distance of $x_{\mathrm{a},k}$ from the nose, each kth accelerometer is affected by pitch acceleration, which contributes to the measurement of rigid body normal acceleration, denoted $n_{\mathrm{z},k}$:

$$n_{\mathrm{z},k} = n_{\mathrm{z}} - \frac{1}{g}(x_{cg} - x_{\mathrm{a},k})\dot{Q}. \tag{4}$$

The flexible states affect normal acceleration as follows:

$$n_{\mathrm{z},f,k} = n_{\mathrm{z},k} + \frac{1}{g} \sum_{i=1}^{n} \bar{\phi}_i(x_{\mathrm{a},k})\ddot{\eta}_i. \tag{5}$$

Currently, normal acceleration is not used as a state within the aircraft's equations of motion, so we add (5) as an output of the plant linearization.

III. Observer Based Output Feedback Control

The first approach we pursue for output-feedback control is to use a classical design based on the separation principle. For this case study, a modified version of the controller developed in Ref. 5 will be used as a baseline certainty-equivalence controller, to be paired with an asymptotic observer employed for state reconstruction. We begin by presenting a linearized plant model and then move on to the design of the controller.

A. State Variable Representation

Previous control work[5, 6] for the Bolender and Doman hypersonic vehicle model has developed the framework for the following discussion of the state variable representation. As opposed to Ref. 5, however, the diffuser-area ratio A_d is not used for control design, and it is therefore kept constant to the value $A_d = 1$. Moreover, an additional control effector (canard) contributes to the vehicle control authority. The eleven-state, three-input nonlinear system (1) is linearized about a trim condition using numerical tools. The resulting linearized model is represented in the familiar form as

$$\begin{aligned}
\dot{x}_p &= A_p x_p + B_p u_p \\
y_p &= C_p x_p + D_p u_p \\
z_p &= H_p x_p,
\end{aligned} \tag{6}$$

State		Input
$V_t = 7846.4$ ft/sec	$\eta_1 = 0.54309$ ft	$\delta_e = 6.5946$ deg
$\alpha = 2.9883$ deg	$\eta_2 = -0.10249$ ft	$\delta_c = -5.6041$ deg
$Q = 0$ deg/sec	$\eta_3 = -0.034697$ ft	$\phi = 0.20739$
$h = 85000$ ft	$\dot{\eta}_i = 0$ ft/sec, $i = 1, 2, 3$	
$\theta = 2.9883$ deg		

Table 2. Trim condition for the linearization of the hypersonic vehicle model. The vehicle is at 50% fuel condition, with vehicle mass $m = 14786$ slug and center of gravity $x_{cg} = 53.8218$.

where the input vector reads as $u_p = [\delta_e, \delta_c, \phi]^T$. The measurement output is given $y_p = [V_t, \alpha, Q_{f,j}, h, n_{z,f,k}]$ (note the feed-forward matrix D_p resulting from the normal acceleration sensor), while the output to be controlled is given by $z_p = [V_t, \gamma]$, where $\gamma := \theta - \alpha$ is the flight path angle (FPA). The trim condition used in this study to derive the model (6) is given in Table 2 The reference commands $r = [V_{\text{ref}}, \gamma_{\text{ref}}]^T$ to be tracked in this setup consist of step functions, smoothed by a second-order pre-filter chosen so that a 1000 ft/s change in velocity V_t settles after approximately 100 seconds, and a 1° change in flight path angle γ transitions after approximately 2 seconds. The reference model with state $x_m \in \mathbb{R}^2$ is written as

$$
\begin{aligned}
\dot{x}_m &= A_m x_m + B_m r \\
z_m &= H_m x_m ,
\end{aligned}
\tag{7}
$$

whereas the tracking error is defined as $e = M_m x_m - H_p x_p$. The model is then augmented by the integral error $x_I = \int_0^t e(\tau)d\tau$. The combined system, with states $x = [x_p^T, x_m^T, x_I^T]^T$ and inputs $u = u_p$, is written as

$$
\begin{aligned}
\dot{x} &= Ax + Bu + Gr \\
y &= Cx + Du \\
e &= Hx,
\end{aligned}
\tag{8}
$$

where the matrices A, B, G, C, D, and H are defined appropriately in accordance with the description above. Note that, as opposed to Ref. 5, the information available for feedback is the measured output y.

B. Output-Feedback Control Design

Considering control design separately from state estimation, the feedback gains are calculated via Linear Quadratic Regulator (LQR) methods. The performance index $\mathcal{J}$ of the system is constructed to represent the weighted sum of error and input energy in the following form:

$$
\mathcal{J} = \frac{1}{2} \int_0^\infty (z^T Q z + u^T R u) dt.
\tag{9}
$$

The selection of the weights has been performed using the implicit model-following approach of Ref. 5. The optimal feedback control law reads as

$$
u = -K_x x + K_r r
\tag{10}
$$

where the feedback gain K_x is computed by solving the continuous steady-state Riccati equation associated with (8) and (9), and the feed-forward gain K_r by imposing the equilibrium condition in steady-state.

The physically available measurements of the aircraft only comprise three of the state variables, so the remaining states must be estimated through the construction of an observer. Note that only the states of system (6) need to be estimated, as the integral error can be reconstructed directly from estimates of x_p. Consequently, the expression of the dynamic observer-feedback controller is given as

$$
\begin{aligned}
\dot{\hat{x}}_p &= A_p \hat{x}_p + B_p u_p + L(y - C_p \hat{x}_p - D_p u_p) \\
u &= -K_x \hat{x} + K_r r,
\end{aligned}
\tag{11}
$$

where $\hat{x} = [\hat{x}_p^T, x_m^T, \hat{x}_I^T]^T$. The gain L is calculated by solving a dual of the LQR control problem (LQE).

| | Observability Condition | Observability Condition |
Eigenvalue	(sensors without flexibility)	(sensors with flexibility)
$-0.49020 - 21.4999i$	1.0506×10^8	5.6480×10^5
$-0.49020 + 21.4999i$	1.0506×10^8	5.6480×10^5
$-1.0771 - 53.7145i$	6.6829×10^8	2.8714×10^6
$-1.0771 + 53.7145i$	6.6829×10^8	2.8714×10^6
$-2.1826 - 108.6927i$	1.2310×10^9	4.1545×10^6
$-2.1826 + 108.6927i$	1.2310×10^9	4.1545×10^6

Table 3. Results of PBH observability tests for the system without rate gyros and accelerometers and observability test with a gyroscope placed at $1ft$ and an accelerometer placed at $99ft$. The values are associated with the flexible states.

C.   Sensor Placement

As it is evident from equations (2) and (5), measurements of pitch rate and normal acceleration are affected by vibrations generated by the flexible dynamics. The modeling of sensor vibrations for rate gyroscope and accelerometer represented a key development, since using simple rigid body sensor model in the hypersonic vehicle state observer proved unsuccessful in simulation for full state reconstruction. The observability of the flexible states system is affected by placement of the sensors. Since the flexible states are used in the certainty-equivalence controller (10), the sensors should not be placed at locations that render the occurrence of the flexible states negligible. For this reason, the role of sensor placement strategy is crucial for output feedback design. A well placed sensor must contain vibratory components that can be used for more accurate state reconstruction.

The Popov-Belevitch-Hautus (PBH) test[18] is used to determine system observability. Traditional controllability and observability tests involving the rank of the controllability and observability matrices proved to be unsuitable for this study, as the plant model is poorly conditioned numerically. The PBH test is more complete and results in a degree of observability, related to the ratio between the smallest nonzero singular value and the largest singular value (condition number) of a certain matrix. Specifically, the test states that the system is observable iff for all eigenvalues λ_i of A,

$$\text{rank}\left(\begin{bmatrix} \lambda_i I_n - A \\ --\,-- \\ C \end{bmatrix}\right) = n. \tag{12}$$

The test has been implemented using numerical tools to verify the observability of the system and its dual was used to verify controllability. In the following sections we will discuss the placement strategies, which are defined by the performance index

$$J \;\; = \;\; \max(\text{cond}(\text{PBH}(\lambda, A_p, C_p))). \tag{13}$$

For a certain sensor placement, we compute the eleven condition numbers of the PBH observability matrices. The performance index J is set to the worst condition number (observability of the third flexible state η_3). The larger the condition number, the worse the degree of observability of a given mode.

1.   Independent Rate Gyroscope and Accelerometer Placement

Inspection of equation (2) shows that a rate gyroscope sensor placed at a dominant mode shape anti-node will minimize the contribution of the flexible term, setting $Q_f \approx Q$. This is a poor choice for an observer because the rate-gyroscope measurement does not contain sufficient information from the flexible states. This location produces an ill-conditioned observability matrix (for example, at $x_{\text{rg},1} = 51.1$ ft in Figure 3(a)). The system outputs will contain richer information from the flexible effects if the rate gyroscope sensors are placed at locations of high $\frac{d\bar{\phi}}{dx}$ values, such as at mode shape nodes for example, at $x_{\text{rg},1} = 30.4$ ft in Figure 3(a)). This effect is seen in Table 3, where observability matrices have maximum order of 10^6 for a well placed sensor suite. The last column in Table 3 represents the improved observability condition numbers for

No. of Sensors	J	Rate Gyroscopes	Accelerometers
2	4.1373×10^6	$x_{\mathrm{rg},1} = 1.0$	$x_{\mathrm{a},1} = 99.0$
3	2.8903×10^6	$x_{\mathrm{rg},1} = 5.4$	$x_{\mathrm{a},1} = 66.5,\ x_{\mathrm{a},2} = 11.9$
3	4.3852×10^6	$x_{\mathrm{rg},1} = 2.7,\ x_{\mathrm{rg},2} = 97.3$	$x_{\mathrm{a},1} = 1.0$
4	2.6488×10^6	$x_{\mathrm{rg},1} = 76.8,\ x_{\mathrm{rg},2} = 14.3$	$x_{\mathrm{a},1} = 88.7,\ x_{\mathrm{a},2} = 12.0$

Table 4. A sample of results for simultaneous placement of multiple rate gyroscopes and accelerometers.

well-placed rate gyroscope and accelerometer sensors. The observability improvement can quickly be seen in the last row, which is initially of order 10^9 and improves to order 10^6 after careful sensor placement. Figure 3(a) shows a single rate gyroscope sensor's effect on observability, plotting J in (13) versus physical location $x_{\mathrm{rg},1}$. The effect of placing a single accelerometer on observability of the flexible stated is shown in Figure 3(b). The peaks of higher unobservability index correlate with low $\frac{d\bar{\phi}}{dx}$ values evaluated along the mode shapes.
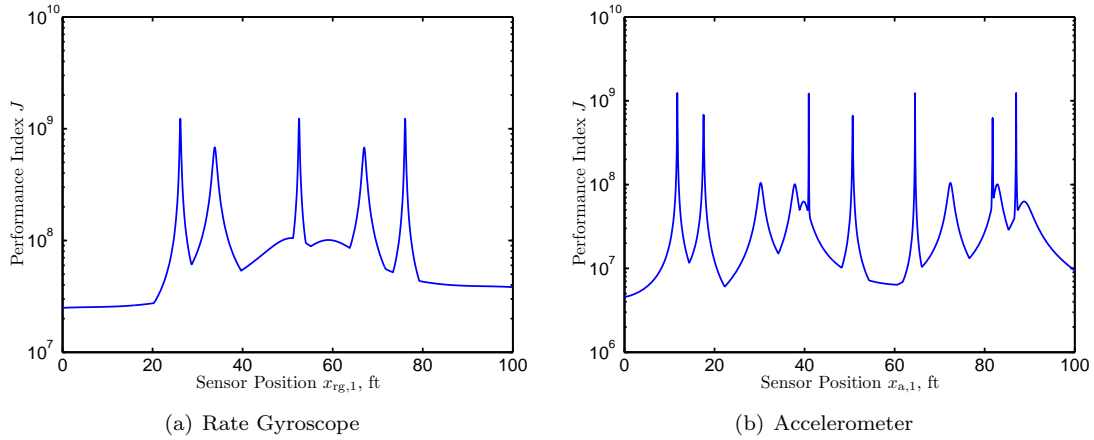

(a) Rate Gyroscope

(b) Accelerometer

Figure 3. Rate gyroscope and accelerometer sensor placement effects on observability at 50% fuel condition.

2. Simultaneous Rate Gyroscope and Accelerometer Placement

Placing multiple rate gyroscopes and accelerometers on the aircraft can best be accomplished through the application of nonlinear constrained optimization. Again, the performance index for this optimization is the maximum observability condition number of the plant from (13). A quasi-Newton algorithm is used for the optimization, consisting of Hessian update and line search procedures. The locations are constrained between the nose and tail of the aircraft; further, shooting methods divide the aircraft into ranges for each sensor to be placed. The mode shapes were provided with resolution of 0.1 ft, so a branch and bound algorithm must also be applied to account for these discrete steps. A sample of the performance index results are listed in Table 4.

The sensor suite chosen for observer simulations in Section D is a rate gyroscope placed at 1 ft, and an accelerometer placed at 99 ft. This choice was made through the aforementioned reasoning for sensor placement strategy, as well as the numerical optimization results contained in Table 4. Adding redundant sensors would reduce the effect of sensor failure, increase controller reliability and increase observability; but this suite of two sensors will provide the baseline for simulations of observer based output feedback control.

D. Simulation Results of Observer Based Output Feedback Control

The nonlinear equations of motion (1) have been implemented in SIMULINK for simulation with the observer-based controller designed for the linearized plant. We consider a default fuel condition as $\frac{1}{2}$ full, with trim condition given in Table 2. The flight path angle reference γ_{ref} is increased by $1°$ from the trim conditions,
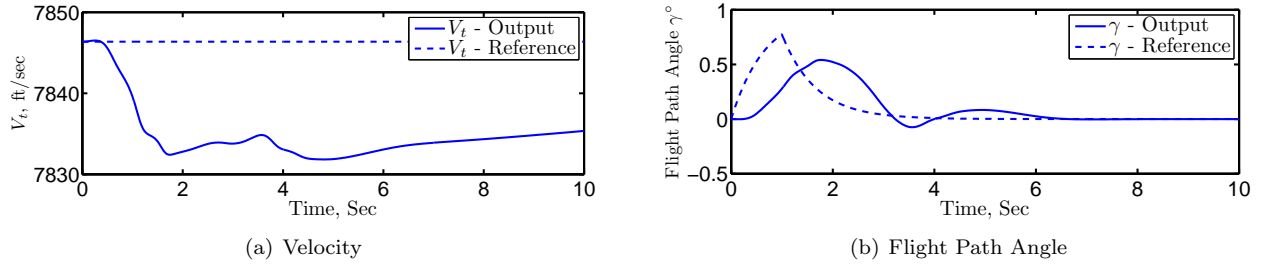
(a) Velocity

(b) Flight Path Angle

Figure 4. Reference trajectories: The vehicle velocity is commanded constant, and the flight path angle is commanded $1°$ up-and-down.

then returned to trim after 2 seconds, while the vehicle velocity V_t is commanded to remain constant at the trim value. The results of the simulation in nominal operating conditions (when the observer model matches
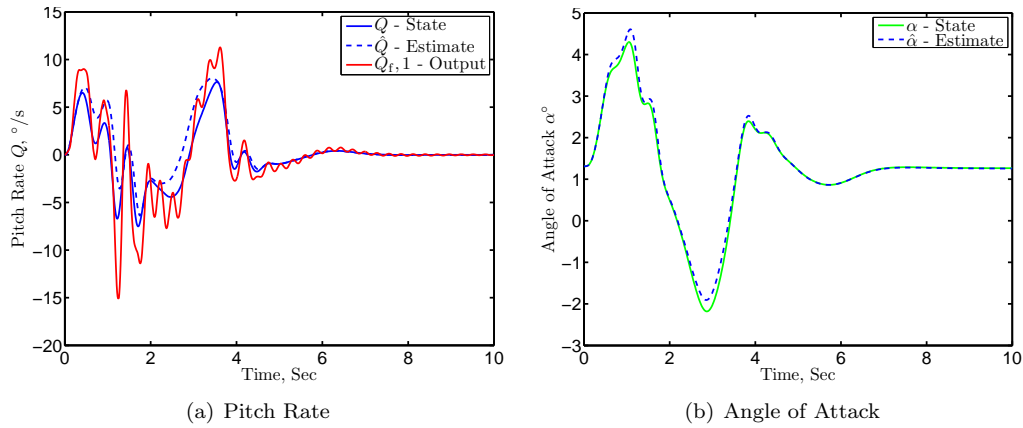

(a) Pitch Rate

(b) Angle of Attack

Figure 5. Pitch rate (a) and angle of attack (b) showing output feedback control results using a gyroscope placed at $1ft$ from the nose and an accelerometer placed at $99ft$.

the linearized vehicle dynamics) reveal a somewhat limited capability of the observer-based controller to achieve tracking of the reference trajectory. In particular, Figure 4, showing the controlled outputs alongside their commanded reference, reveals that stability is maintained in closed-loop and that the tracking error converges to zero asymptotically after a sizable transient. Figure 5(a) shows the rate gyroscope measurement Q_f, the actual state trajectory Q, and the reconstructed state trajectory $\hat{Q}$. The angle of attack estimate $\hat{\alpha}$ is also compared with its actual trajectory α in Figure 5(b). The remaining states are successfully reconstructed with similar results. The linear observer-based controller, however, shows poor robustness to plant variations. Commanding a typical change in velocity of 1000 ft/sec results in inaccurate state estimates that destabilize the system, as seen in Figure 6. Such a change invalidates the linearization to the point that a new linearization for the observer must be computed. The closed-loop system is also sensitive to parameter variations, namely to changes in fuel conditions. The baseline linear observer designed for a $\frac{1}{2}$ full fuel condition is simulated with a plant trimmed at empty fuel condition in Figure 7(a). The state estimates do not converge to the true state values due to this system uncertainty, and the inaccurate estimates destabilize the system. Instability also occurs for a simulation with a full-fuel model, as shown in Figure 7(b).

IV.   Robust Output Feedback Control

The poor robustness exhibited by the linear observer-based controller, which could not be mitigated by a different selection of the weights of the LQR/LQE problem, motivated a further investigations into robust output feedback methods that do not rely on an observer. By writing the linearized system in normal form we observe that the unstable zero-dynamics with respect to the I/O pair $(\phi, \delta_e)/(V_t, h)$ can be compensated by means of an auxiliary robust dynamic controller which, driven by the output Q_f, commands the input
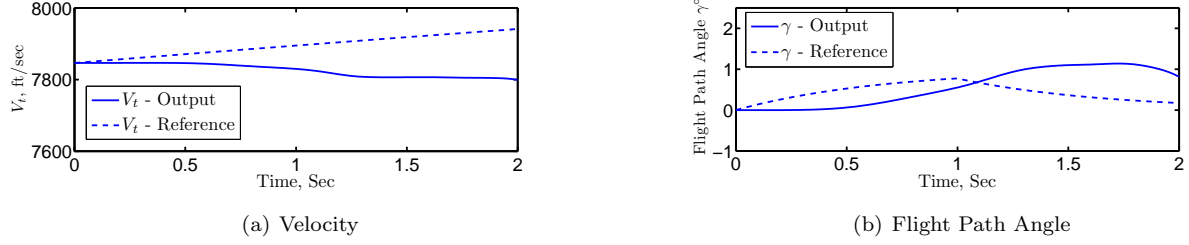
(a) Velocity

(b) Flight Path Angle

Figure 6. Observer failure: The baseline reference trajectory is modified so that velocity is commanded to increase by 1000 ft/s. The flight path angle reference trajectory is unmodified from the command of 1° up-and-down.
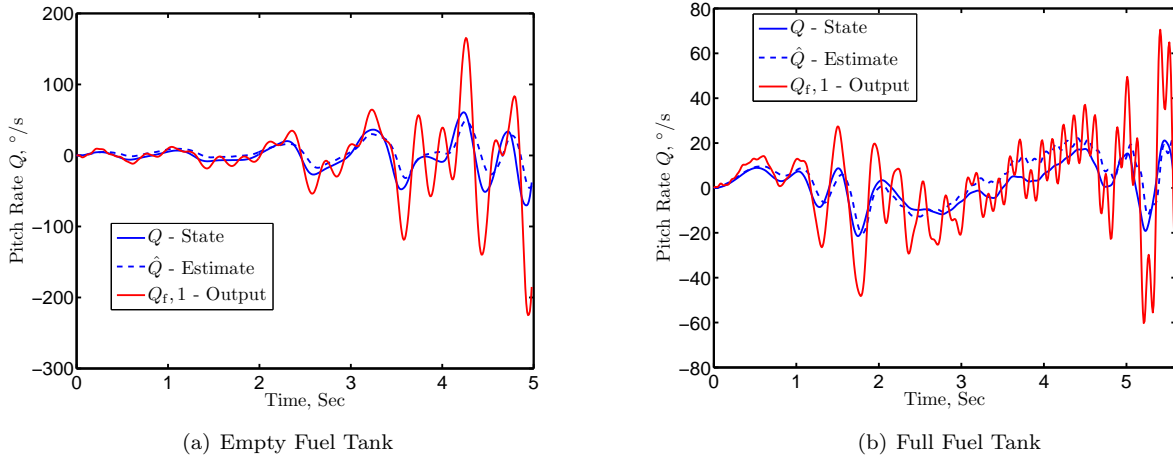

(a) Empty Fuel Tank

(b) Full Fuel Tank

Figure 7. Observer failure: Baseline observer designed for half full fuel tank and (a) Simulated for an empty fuel tank plant, (b) Simulated for a full fuel tank. Gyroscope placed 1 ft from the nose and accelerometer placed at 99 ft.

δ_c. The zero-dynamics include the unstable pitch dynamics and the stable dynamics of the flexible states. The auxiliary controller is designed to be robust with respect to parameter variations due changes in the fuel condition. Since the position of the rate gyro sensor affects the position of the transmission zeros of the zero dynamics, sensor placement plays a major role in the implementation of the auxiliary controller. After the zero-dynamics have been compensated, servomechanism theory is employed to design a partial-state feedback controller achieving robust tracking of reference trajectories for the vehicle velocity and altitude. Time-scale separation and composite control methods are used to alleviate the complexity of the design.

A. Linearized Vehicle Model

The dynamics of the flexible vehicle model linearized about a trim condition are re-written as

$$\begin{aligned}
\dot{x}_r &= A_{11}(\mu)x_r + A_{12}(\mu)x_f + B_1(\mu)u \\
\dot{x}_f &= A_{21}(\mu)x_r + A_{22}(\mu)x_f + B_2(\mu)u \\
y &= C_1 x_r + C_2(\mu)x_f \,,
\end{aligned} \tag{14}$$

where x_r is the rigid-body state, x_f is the flexible state, $u = [\phi, \delta_e, \delta_c]^T$ is the control input, and $y = [V_t, h, Q_f]^T$ is the measured output. Measurements of the normal acceleration have not been included in the output vector, due to their sensitivity on the operating conditions. The vector $\mu \in \mathbb{R}^p$ denotes uncertain parameters due to the trim, the position of the rate gyro sensor, and other plant parameters such as the

fuel level. The actual value of μ is not known, but μ is assumed to range over a given compact set $\mathcal{P} \subset \mathbb{R}^p$, which depends on the flight envelope. It is assumed that only one rate gyro sensor is employed. Finally, the output to be controlled is chosen as $\bar{y} = [V_t, h]^T$, where the altitude h replaced the flight-path angle γ. The following facts hold for the plant model, for any $\mu \in \mathcal{P}$:

1. The system (14) has vector relative degree $r = \{1, 2\}$ with respect to the regulated output $\bar{y}$ and the control input u.

2. Any combination of two different control inputs among the three available in u results in unstable zero dynamics with respect to $\bar{y}$. In particular, choosing $\bar{u} = (\phi, \delta_e)$, the resulting 8-dimensional zero-dynamics with respect to $\bar{y}$ possess 3 pairs of complex conjugate eigenvalues in $\text{Re}[\lambda] < 0$ (due to the flexible effects) and a pair of real eigenvalues (due to the pitch/pitch rate dynamics,) located symmetrically with respect to the imaginary axis.

1.   Normal Form & Zero-Dynamics

Denote with $u_{\text{aux}} \in \mathbb{R}$ and $y_{\text{aux}} \in \mathbb{R}$ the auxiliary input and the auxiliary output of system (14), given respectively by $u_{\text{aux}} = \delta_c$ and $y_{\text{aux}} = Q_f$, and change coordinates as $(x_r, x_f) \to (x, \bar{\eta})$, where

$$x = [V_t, h, \dot{h}]^T, \qquad \bar{\eta} = [\eta^T, \dot{\eta}^T, \theta, Q]^T$$

and $\dot{h}$ replaces α as a state of the system. Thus, we obtain the system

$$
\begin{aligned}
\dot{x} &= \bar{A}_{11}(\mu)x + \bar{A}_{12}(\mu)\bar{\eta} + B_{11}(\mu)\bar{u} + B_{12}(\mu)u_{\text{aux}} \\
\dot{\bar{\eta}} &= \bar{A}_{21}(\mu)x + \bar{A}_{22}(\mu)\bar{\eta} + B_{21}(\mu)\bar{u} + B_{22}(\mu)u_{\text{aux}} \\
\bar{y} &= \bar{C}_{11}x \\
y_{\text{aux}} &= \bar{C}_{22}(\mu)\bar{\eta}.
\end{aligned}
\tag{15}
$$

The triplet $(\bar{A}_{11}, \bar{B}_{11}, \bar{C}_{11})$ has the following structure

$$
\bar{A}_{11}(\mu) = \begin{pmatrix} \bar{a}_{11} & \bar{a}_{12} & \bar{a}_{13} \\ 0 & 0 & 1 \\ \bar{a}_{31} & \bar{a}_{32} & \bar{a}_{33} \end{pmatrix}, \qquad
B_{11}(\mu) = \begin{pmatrix} b_{11} & b_{12} \\ 0 & 0 \\ b_{31} & b_{32} \end{pmatrix}, \qquad
\bar{C}_{11} = \begin{pmatrix} 1 & 0 & 0 \\ 0 & 1 & 0 \end{pmatrix},
$$

where the matrix

$$
\mathcal{B}(\mu) = \begin{pmatrix} b_{11} & b_{12} \\ b_{31} & b_{32} \end{pmatrix}
\tag{16}
$$

is non-singular. In particular, it is assumed that a number $b_{11}^0 > 0$ is known such that $b_{11}(\mu) \geq b_{11}^0$ for all $\mu \in \mathcal{P}$. Moreover, since it can be shown that $\text{Im}\,\bar{A}_{12} \subset \text{Im}\,B_{11}$, the matrix $\bar{A}_{12}$ has the following structure

$$
\bar{A}_{12}(\mu) = \begin{pmatrix} * & \dots & * \\ 0 & \dots & 0 \\ * & \dots & * \end{pmatrix},
$$

where '*' denotes unspecified (possibly non-zero) entries. Changing coordinates again using

$$
z = \bar{\eta} - B_{21}(\mu)\mathcal{B}^{-1}(\mu) \begin{pmatrix} x_1 \\ x_3 \end{pmatrix}
$$

and rearranging variables, the system is put in *normal form*

$$
\begin{aligned}
\dot{z} &= F(\mu)z + G(\mu)u_{\text{aux}} + J_{11}(\mu)x \\
\dot{x} &= A(\mu)x + B(\mu)\bar{u} + J_{21}(\mu)z + J_{22}(\mu)u_{\text{aux}} \\
\bar{y} &= Cx \\
y_{\text{aux}} &= H(\mu)z + J_{12}(\mu)x
\end{aligned}
\tag{17}
$$

where $B(\mu) = \bar{B}_{11}(\mu)$, $C = \bar{C}_{11}$, and

$$A(\mu) = \begin{pmatrix} a_{11} & a_{12} & a_{13} \\ 0 & 0 & 1 \\ a_{31} & a_{32} & a_{33} \end{pmatrix}, \quad J_{21}(\mu) = \begin{pmatrix} * & \dots & * \\ 0 & \dots & 0 \\ * & \dots & * \end{pmatrix}, \quad J_{22}(\mu) = \begin{pmatrix} * \\ 0 \\ * \end{pmatrix}.$$

It is well known that the eigenvalues of $F(\mu)$ are exactly the transmission zeros of the original system (between the input $\bar{u}$ and the output $\bar{y}$.) Due to the structure of the triplet (A, B, C), and the fact that $\mathrm{Im}\,[J_{21}\ J_{22}] \subset \mathrm{Im}\,B$, the zero dynamics of the system are given by the trajectories of the controlled system

$$\begin{aligned} \dot{z} &= F(\mu)z + G(\mu)u_{\mathrm{aux}} \\ y_{\mathrm{aux}} &= H(\mu)z \,. \end{aligned} \tag{18}$$

It can be verified that system (18) is both controllable and observable for almost all $\mu \in \mathcal{P}$, except for certain singular positions of the rate gyro sensor, where observability of some flexible state is lost.

B. Robust Stabilization of the Zero-Dynamics

Since the triplet (F, G, H) is controllable and observable, it is possible to design a dynamic output feedback controller to stabilize the zero dynamics system (18). However, this must be accomplished in spite of the parameter uncertainty, and thus a standard approach based on state observation may lead to poor robustness. A closer look at the structure of (18) reveals that the system in question has relative degree one and is weakly non-minimum phase, in the sense that all zeros are in $\mathrm{Re}[\lambda] \leq 0$, with a simple zero at the origin. In particular, the pole/zero structure of the zero-dynamics for the nominal trim condition is depicted in Fig. 8. In particular, note the pole/zero interlacing property due to the flexible dynamics, and
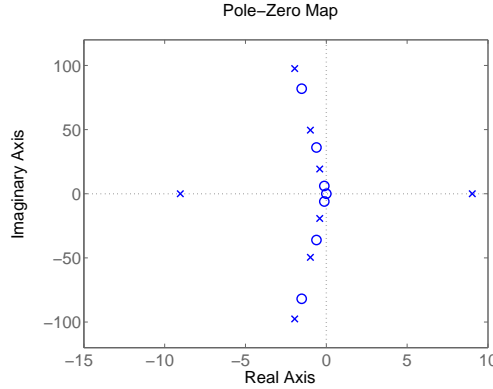

Figure 8. Pole/zero structure of the controlled zero dynamics (18).

the presence of the zero at the origin, due to the fact that the auxiliary output y_{aux} is a linear combination of pitch rate and derivatives of the flexible modes. Changing the position of the rate gyro sensor will affect the position of the complex zeros. The important issue of sensor placement will be addressed in the next section.

Any static output feedback of the form $u_{\mathrm{aux}} = -k\,y_{\mathrm{aux}}$, $k > 0$ results in an unstable closed-loop, as the right-hand side pole migrates towards the zero at the origin. However, the positive feedback interconnection with a simple dynamic compensator of the form

$$K_a(s) = -\kappa \frac{s + \beta}{s - \gamma}, \qquad \kappa > 0,\ \beta > 0,\ \gamma > 0 \tag{19}$$

results in a stable closed loop system if γ and β are suitably chosen smaller that the magnitude of the unstable pole, and κ is large enough. Moreover, if the structure of the pole/zero map of (18) is preserved when μ varies within the compact set $\mathcal{P}$, the simple dynamic controller provides robust stabilization. Figure 9(a) shows an example of the root locus of the controlled zero-dynamics, whereas Figure 9(b) shows the variation

American Institute of Aeronautics and Astronautics
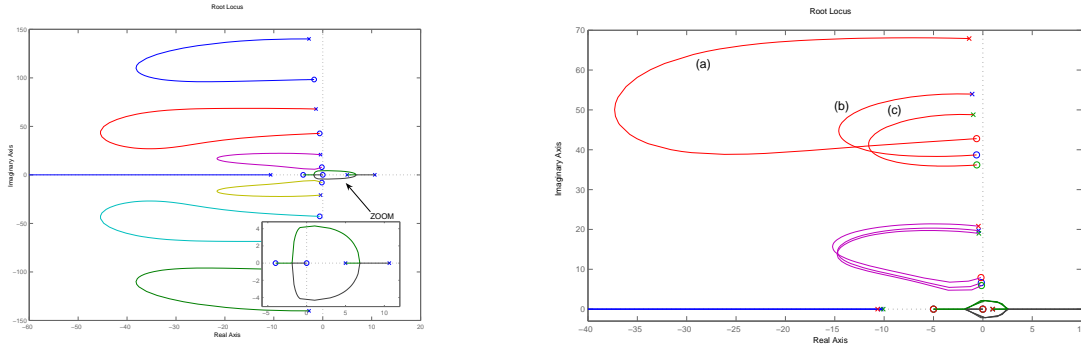
(a) Root locus of the compensated zero dynamics.   (b) Root locus of the compensated zero dynamics. Variations in fuel level: (a) empty tank, (b) half-full tank, (c) full tank.

Figure 9. Root loci of the compensated zero dynamics.

of the root locus due to changes in fuel tank from full (a) to empty (c). It can be noted that the same controller stabilizes all three configurations. The robust compensator (19) has a state-space realization

$$
\begin{aligned}
\dot{\xi}_0 &= \gamma\xi_0 + (\beta + \gamma)y_{\text{aux}} \\
u_{\text{aux}} &= -\kappa\xi_0 - \kappa y_{\text{aux}}
\end{aligned}
\tag{20}
$$

with state $\xi_0 \in \mathbb{R}$, yielding the augmented internal dynamics

$$
\begin{aligned}
\dot{z}^a &= F^a(\mu)z^a + J_1^a(\mu)x \\
\dot{x} &= A^a(\mu)x + J_2^a(\mu)z^a + B(\mu)\bar{u} \\
\bar{y} &= C\,x
\end{aligned}
\tag{21}
$$

where $z^a = [\xi_0, z^T]^T$, and $F^a(\mu)$, $A^a(\mu)$, $J_1^a(\mu)$, and J_2^a are defined appropriately.

1.   Sensor Placement for Robust Compensation of the Zero-Dynamics

As mentioned above, placement of the rate gyro affects the position of the complex zeros of system (18). Moving the sensor from the front of the vehicle towards the back causes the zeros to migrate upwards and pass through the poles. Since the sensor is placed at a fixed position, it is desirable to obtain a pole-zero structure that remains favorable for robust stabilization for any fuel level and flight condition within the flight envelope. By a favorable pole-zero structure we mean that the angles of departure of the complex
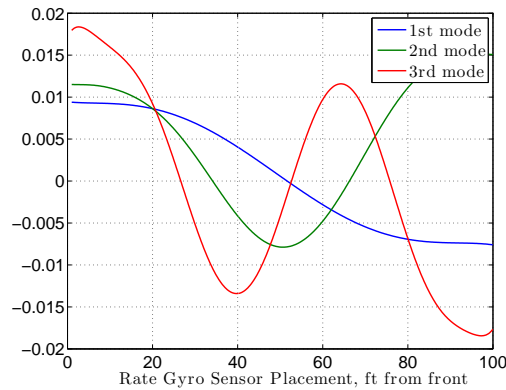

Figure 10. Mass normalized flexible mode shapes derivatives for a specific flight condition and vehicle parameters.

(a) Root loci for the compensated zero dynamics for
two fixed μ, the rate gyro sensor placed at either 25ft
or 30ft from the front.

(b) Root locus of the compensated zero dynamics.
Variations include 5 different flight conditions from
$V_t = 7846$ft/s-8846ft/s, $h = 85000$ft-95000ft, and 2
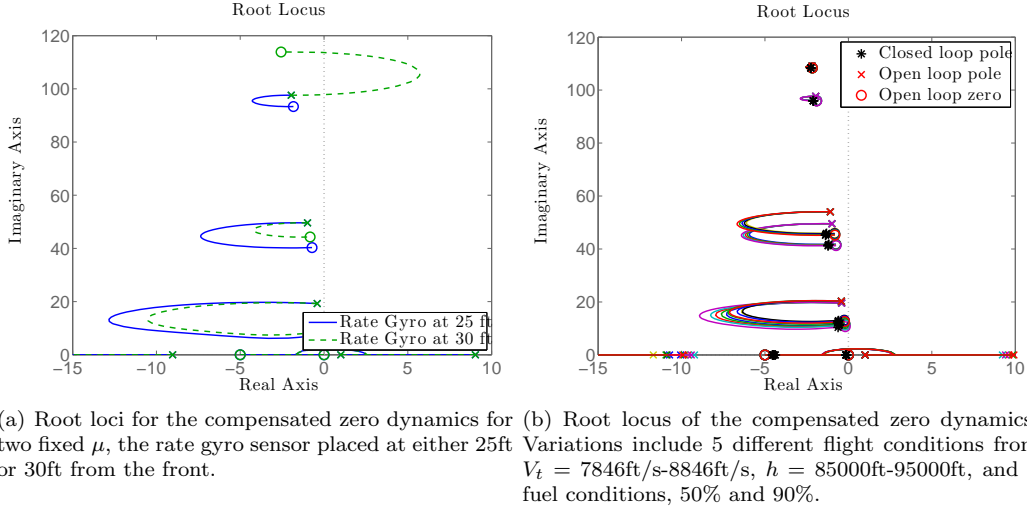fuel conditions, 50% and 90%.

Figure 11. Root loci of the compensated zero dynamics & sensor placement

roots of the zero dynamics with the auxiliary compensator are towards the left. As seen on figure 11(a), if
the sensor is placed passed a certain position, the angle of departure for the third flexible mode derivative
turns towards the right. The exact position of this point depends on the mode shapes of the flexibility and
thus on the fuel level. Furthermore, we seek to minimize the effect of the flexible states on the output Q_f,
thus providing a better estimate of Q and reducing oscillations in our canard control commands due to the
flexible states. In this respect, it would be ideal to place the sensor at common node for all the mode shapes
of the flexible state derivatives. Nodes correspond to pole-zero cancellations in the zero-dynamics and thus
to unobservability of the respective flexible mode from Q_f. However, as we see from figure 10, the modes
do not posses a common node. Consequently, we have chosen to place the sensor such that we minimize
a weighted norm of the mode shapes of the flexible state derivatives while maintaining conservatively a
favorable pole-zero structure of the zero dynamics for any fuel level and flight condition within the flight
envelope, as described above.

C. Filtered Transformation

Once the internal dynamics have been rendered asymptotically stable, a viable strategy to stabilize the
overall system (21) is to enforce, via $\bar{u}$, a small-gain interconnection using feedback from the partial state
x. Note, however, that the state x is not available for feedback. For this reason, a preliminary dynamic
transformation is needed to obtain a system that is in the required form for partial-state feedback control.
To avoid differentiating the second component of the output, a so-called filtered transformation is employed.
For convenience of notation, let $\bar{u} = [u_1, \ u_2]^T = [\phi, \ \delta_e]^T$, $\bar{y} = [y_1, \ y_2]^T = [V_t, \ h]$, and augment the
dynamics (21) with the scalar system

$$\dot{\xi}_1 = -\lambda \xi_1 + u_2 \tag{22}$$

where $\lambda > 0$ is a design parameter. Next, applying the change of coordinates

$$\bar{x}_3 = x_3 - \frac{b_{31}}{b_{11}} x_1 + \frac{b_{31}b_{12} - b_{32}b_{11}}{b_{11}} \xi_1$$

and defining the state of the "extended zero dynamics" as $z^e = [z^{aT}, \bar{x}_3]^T$, one obtains the system

$$\begin{aligned}
\dot{z}^e &= F^e(\mu)z^e + J^e_{11}(\mu)\bar{y} + J^e_{12}(\mu)\xi_1 \\
\dot{\bar{y}} &= A^e_{11}(\mu)\bar{y} + A^e_{12}(\mu)\xi_1 + J^e_2(\mu)z^e + B(\mu)\bar{u} \\
\dot{\xi}_1 &= -\lambda \xi_1 + u_2 \, .
\end{aligned} \tag{23}$$

American Institute of Aeronautics and Astronautics

In particular, the matrix $A_{12}^e(\mu)$ has the structure

$$A_{12}^e(\mu) = \begin{pmatrix} * \\ \frac{b_{31}b_{12} - b_{32}b_{11}}{b_{11}} \end{pmatrix},$$

where $\frac{b_{31}b_{12} - b_{32}b_{11}}{b_{11}} \neq 0$, since $\mathcal{B}(\mu)$ in (16) is non-singular. As a result, the further change of coordinates

$$\bar{z}^e = z^e - \frac{b_{11}}{b_{31}b_{12} - b_{32}b_{11}} J_{12}^e(\mu) x_2, \qquad \bar{x} = [x_1, x_2, \xi_1]^T$$

yields a system in the form

$$
\begin{aligned}
\dot{\bar{z}}^e &= \bar{F}^e(\mu)\bar{z}^e + \bar{J}_1^e(\mu)\bar{y} \\
\dot{\bar{x}} &= \bar{A}^e(\mu)\bar{x} + \bar{J}_2^e(\mu)\bar{z}^e + \bar{B}^e(\mu)\bar{u} \\
\bar{y} &= \bar{C}^e \bar{x},
\end{aligned}
\tag{24}
$$

where $\bar{F}^e(\mu)$ is Hurwitz for any $\mu \in \mathcal{P}$, and the triplet $(\bar{A}^e, \bar{B}^e, \bar{C}^e)$ has the following structure:

$$\bar{A}^e(\mu) = \begin{pmatrix} \bar{a}_{11}^e & \bar{a}_{12}^e & \bar{a}_{13}^e \\ \bar{a}_{21}^e & \bar{a}_{22}^e & \bar{a}_{23}^e \\ 0 & 0 & -\lambda \end{pmatrix}, \quad \bar{B}^e(\mu) = \begin{pmatrix} b_{11} & b_{12} \\ 0 & 0 \\ 0 & 1 \end{pmatrix}, \quad \bar{C}^e = \begin{pmatrix} 1 & 0 & 0 \\ 0 & 1 & 0 \end{pmatrix}.$$

It can be shown that $\bar{a}_{23}^e(\mu) \neq 0$ for all $\mu \in \mathcal{P}$ such that the matrix in (16) is invertible. Without loss of generality, assume $\bar{a}_{23}^e(\mu) > 0$. Note that the upper subsystem (the new internal dynamics with state $\bar{z}^e$) is interconnected to the lower subsystem only via the regulated output $\bar{y}$.) Furthermore, the partial state $\bar{x}$ is now available for feedback. Note that rearranging the order of the state variables as (x_2, ξ_1, x_1) has the effect of highlighting a triangular structure exhibited by the system. The triangular structure suggests a hierarchical approach to the control design. Specifically, the inner chain of integrators (x_2, ξ_1) corresponding to the extended altitude dynamics should be controlled via $u_2 = \delta_e$ on a faster time scale than the dynamics for V_t, which is controlled primarily via $u_1 = \phi$. In regard to this, note that the *zero dynamics of* (24) *with respect to the input/output pair* (u_1, y_1) is given by the controlled system

$$
\begin{aligned}
\dot{\bar{z}}^e &= \bar{F}^e(\mu)\,\bar{z}^e + \bar{J}_{12}^e(\mu)\,x_2 \\
\dot{x}_2 &= \bar{J}_{22}^e(\mu)\,\bar{z}^e + \bar{a}_{22}^e(\mu)\,x_2 + \bar{a}_{23}^e(\mu)\,\xi_1 \\
\dot{\xi}_1 &= -\lambda \xi_1 + u_2 \\
y_2 &= x_2
\end{aligned}
\tag{25}
$$

which has relative-degree two with respect to the I/O pair u_2/y_2, transmission zeros in $\mathrm{Re}[s] < 0$ (the eigenvalues of $\bar{F}^e(\mu)$), and partial state (x_2, ξ_1) available for feedback. Once a robust output-feedback controller $\mathcal{K}_2$ for (25) has been designed, the task becomes that of designing a controller $\mathcal{K}_1$ for the relative degree one- minimum-phase system with input u_1, output x_1, as shown in Figure 12.

D. Robust Servomechanism Approach

In this section, we consider the problem of designing a robust regulator for the system (24). The problem is that of letting $\bar{y}(t)$ asymptotically track a given reference signals $r(t)$. As before, we let $r(t)$ be the output of a decoupled 2$^{\text{nd}}$ order reference model driven by step inputs; consequently, $r(t)$ can be generated as the output of the autonomous system

$$
\begin{aligned}
\dot{w} &= Sw \\
r &= Qw
\end{aligned}
\tag{26}
$$

where $w = [w_1^T, w_2^T]^T \in \mathbb{R}^6$, $r = [r_1, r_2]^T \in \mathbb{R}^2$,

$$S = \begin{pmatrix} S_1 & 0 \\ 0 & S_2 \end{pmatrix}, \quad Q = \begin{pmatrix} Q_1 & 0 \\ 0 & Q_2 \end{pmatrix}, \quad S_i = \begin{pmatrix} 0 & 1 & 0 \\ -\omega_{n,i}^2 & -2\zeta_i\omega_{n,i} & \omega_{n,i}^2 \\ 0 & 0 & 0 \end{pmatrix}, \quad Q_i = \begin{pmatrix} 1 & 0 & 0 \end{pmatrix}, \quad i = 1, 2$$

and $(\zeta_i, \omega_{n,i})$ are respectively the damping ratio and the natural frequency of the i-th reference model.
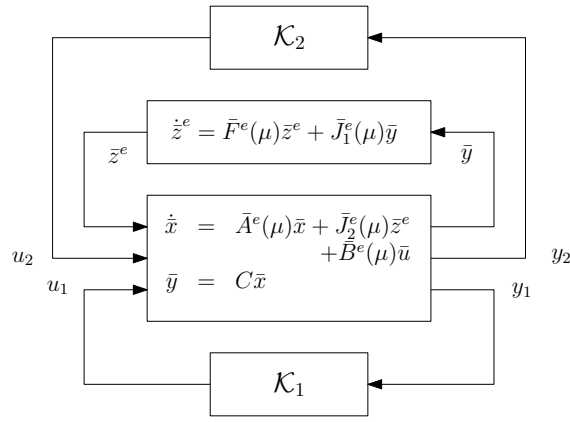
Figure 12. Inner and outer-loop control

1. Inner-loop Design

Consider again the expression of (25), augmented with the reference model for x_2. Assuming that the roots of the Hurwitz polynomial $p_{S_2}(s) = s^2 + 2\zeta\omega_n s + \omega_n^2$ are chosen to be different from the eigenvalues of $\bar{F}^e(\mu)$, there exists a unique parameter dependent solution $\Pi_2(\mu)$ of the Sylvester equation

$$\Pi_2(\mu)S_2 = \bar{F}^e(\mu)\Pi_2(\mu) + \bar{J}_{12}^e(\mu)Q_2 \,.$$

Then, the change of coordinates

$$e_2 = x_2 - r_2 \,, \qquad \tilde{z}^e := \bar{z}^e - \Pi(\mu)w$$

representing respectively the tracking error and a set of transversal coordinates to the zero dynamics of the above system with respect to e_2, yields the *error system*

$$
\begin{aligned}
\dot{w}_2 &= S_2 w_2 \\
\dot{\tilde{z}}^e &= \bar{F}^e(\mu)\,\tilde{z}^e + \bar{J}_{12}^e(\mu)\,e_2 \\
\dot{e}_2 &= \bar{J}_{22}^e(\mu)\,\tilde{z}^e + \bar{a}_{22}^e(\mu)\,e_2 + \bar{a}_{23}^e(\mu)\big[\xi_1 - R_2(\mu)w\big] \\
\dot{\xi}_1 &= -\lambda\,\xi_1 + u_2
\end{aligned}
\tag{27}
$$

where

$$R_2(\mu) = \frac{1}{\bar{a}_{23}^e(\mu)}\big[\bar{J}_{22}^e(\mu)\Pi_2(\mu) + \bar{a}_{22}^e(\mu)Q_2 - Q_2 S_2\big] \,.$$

Note that in order to enforce invariance of $e_2 = 0$, the state ξ_1 must be steered to the steady state trajectory $\xi_1^\star(t) = R_2(\mu)w(t)$, which is not available since μ is not known.

2. Two-time Scale Internal Model Design

Assume, without loss of generality, that the pair $(R_2(\mu), S_2)$ is observable for all $\mu \in \mathcal{P}$. Then, the pair is topologically equivalent to the pair $(Q_2, \bar{S}_2)$, where

$$
\bar{S} = \begin{pmatrix} 0 & 1 & 0 \\ 0 & 0 & 1 \\ 0 & -\omega_n^2 & -2\zeta\omega_n \end{pmatrix} \,.
$$

As a matter of fact, it is easy to see that $S_2 = \Theta_2^{-1}(\mu)\bar{S}_2\Theta_2(\mu)$ and $R_2(\mu) = Q_2\Theta_2(\mu)$, where $\Theta_2(\mu)$ is the observability matrix of $(R_2(\mu), S_2)$. It should be emphasized that while the pairs $(R_2(\mu), S_2)$ and $(Q_2, \bar{S}_2)$ are equivalent representation of the same autonomous system, the latter is independent of the uncertain parameter μ. This result is exploited for the construction of an internal model of the uncertain steady state trajectories of (27) compatible with the condition $e_2 = 0$.

American Institute of Aeronautics and Astronautics

The goal of the inner-loop control is (i) to enforce by feedback an invariant subspace for the system (27), in which the tracking error is identically zero; (ii) to render the subspace in question globally attractive; (iii) to induce a time-scale separation between the $\tilde{z}^e$-dynamics and the dynamics of the tracking error e_2. To begin with, denote with $\rho > 0$ an adjustable high-gain parameter, and let $\varepsilon = 1/\rho$. Let (Σ_2, Ξ_2) be the pair in controller form

$$\Sigma_2 = \begin{pmatrix} 0 & 1 & 0 \\ 0 & 0 & 1 \\ -\sigma_0 & -\sigma_1 & -\sigma_2 \end{pmatrix}, \qquad \Xi_2 = \begin{pmatrix} 0 \\ 0 \\ 1 \end{pmatrix} \tag{28}$$

where the coefficients of the Hurwitz polynomial $p_{\Sigma_2}(s) = s^3 + \sigma_2 s^2 + \sigma_1 s + \sigma_0$ are chosen arbitrarily, in such a way that the roots of $p_{\Sigma_2}(s)$ are distinct from those of the polynomial $p_S(s)$. Then, for any $\rho > 0$ there exists a unique solution $M_2(\rho)$ of the Sylvester equation

$$M_2(\rho)\bar{S} = \rho\Sigma_2 M_2(\rho) + \Xi_2 Q_2 \tag{29}$$

which is also nonsingular. Post-multiplying both sides of equation (29) by $M_2^{-1}(\rho)$, one obtains

$$M_2(\rho)\bar{S}M_2^{-1}(\rho) = \rho\Sigma_2 + \Xi_2\Psi_2(\rho)$$

where $\Psi_2(\rho) := Q_2 M_2^{-1}(\rho)$. It is readily seen that $\Psi_2(\rho)$ is the unique feedback matrix that assigns to the pair $(\rho\Sigma_2, \Xi_2)$ the eigenvalues of $\bar{S}$, so the expression of $\Psi_2(\rho)$ can be easily computed as

$$\Psi_2(\rho) = \rho\bar{\Psi}_2(\varepsilon), \qquad \bar{\Psi}_2(\varepsilon) := \begin{pmatrix} -\sigma_0 & -\sigma_1 + \varepsilon^2\omega_n^2 & -\sigma_2 + 2\varepsilon\zeta\omega_n \end{pmatrix}. \tag{30}$$

In particular, note that $\bar{\Psi}_2(\varepsilon) = \mathcal{O}(1)$. A candidate internal model for the steady-state trajectory $\xi_1^\star(t) = R_2(\mu)w(t) = Q_2\Theta_2(\mu)w(t)$ is constructed as the one-parameter family of dynamical systems

$$\begin{aligned} \dot{\xi}_2 &= \rho\Sigma_2\xi_2 + \Xi_2\xi_1 \\ \upsilon &= \Psi_2(\rho)\xi_2. \end{aligned} \tag{31}$$

Augmenting the system (27) with the internal model (31), changing coordinates as

$$\tilde{\xi}_1 := \xi_1 - \Psi_2(\rho)\xi_2$$
$$\tilde{\xi}_2 := \xi_2 - M_2(\rho)\Theta_2^{-1}(\mu)w - \frac{1}{\bar{a}_{23}^e(\mu)}\Xi_2 e_2,$$

and rearranging terms after some manipulations, one obtains the system

$$\begin{aligned} \dot{\tilde{z}}^e &= \bar{F}^e(\mu)\,\tilde{z}^e + \bar{J}_{12}^e(\mu)\,e_2 \\ \dot{e}_2 &= \bar{J}_{22}^e(\mu)\,\tilde{z}^e + \left[\bar{a}_{22}^e(\mu) + \Psi_2(\rho)\Xi_2\right]e_2 + \bar{a}_{23}^e(\mu)\tilde{\xi}_1 + \bar{a}_{23}^e(\mu)\Psi_2(\rho)\tilde{\xi}_2 \\ \dot{\tilde{\xi}}_1 &= -\lambda\xi_1 - \Psi_2(\rho)\left[\rho\Sigma_2\xi_2 + \Xi_2\xi_1\right] + u_2 \\ \dot{\tilde{\xi}}_2 &= \rho\Sigma_2\tilde{\xi}_2 - \frac{1}{\bar{a}_{23}^e(\mu)}\Xi_2\bar{J}_{22}^e(\mu)\tilde{z}^e + \frac{1}{\bar{a}_{23}^e(\mu)}\left[\rho\Sigma_2 - \bar{a}_{22}^e I\right]\Xi_2 e_2. \end{aligned} \tag{32}$$

Note that, for reasons that will become clear in a moment, we have kept the original coordinates ξ_1, ξ_2 in the expression of the dynamics of $\tilde{\xi}_1$. Since the state variables of the dynamic extension and the internal model are available for feedback, and so is the partial state $(e_2, \tilde{\xi}_1)$, the control u_2 can be selected as the "feedforward plus partial-state feedback"

$$u_2 = \left[\lambda_1 + \Psi_2(\rho)\Xi_2\right]\xi_1 + \rho\Psi_2(\rho)\Sigma_2\xi_2 - \rho\,k^2 e_2 - \rho k\,\tilde{\xi}_1 \tag{33}$$

where $k > 0$ is a scalar gain parameter. Letting $\chi_2 = \text{col}\,(e_2, \tilde{\xi}_1, \tilde{\xi}_2)$, and dividing the corresponding dynamics with ρ, system (32) in closed loop with (33) is conveniently written as a singular perturbation model in standard form

$$\begin{aligned} \dot{\tilde{z}}^e &= \bar{F}^e(\mu)\,\tilde{z}^e + \bar{J}_{12}^e(\mu)C_2\chi_2 \\ \varepsilon\dot{\chi}_2 &= A_2(\mu, \varepsilon, k)\chi_2 + \varepsilon B_2(\mu)\tilde{z}^e, \end{aligned} \tag{34}$$

where

$$A_2(\mu,\varepsilon,k) = \begin{pmatrix} \varepsilon\bar{a}_{22}^e(\mu) + \bar{\Psi}_2(\varepsilon)\Xi_2 & \varepsilon\bar{a}_{23}^e(\mu) & \bar{a}_{23}^e(\mu)\bar{\Psi}_2(\varepsilon) \\ -k^2 & -k & 0 \\ \frac{1}{\bar{a}_{23}^e(\mu)}\Sigma_2\Xi_2 - \varepsilon\bar{a}_{22}^e(\mu)\Xi_2 & 0 & \Sigma_2 \end{pmatrix},$$

and

$$B_2(\mu) = \begin{pmatrix} \bar{J}_{22}^e(\mu) \\ 0 \\ -\frac{1}{\bar{a}_{23}^e(\mu)}\Xi_2\bar{J}_{22}^e(\mu) \end{pmatrix}, \qquad C_2 = \begin{pmatrix} 1 & 0 & 0 \end{pmatrix}.$$

Proposition IV.1 *There exists $k^\star > 0$ such that for any given $k \geq k^\star$ the matrix $A_2(\mu,\varepsilon,k)$ is Hurwitz for all $\mu \in \mathcal{P}$ and all $\varepsilon \in (0,1]$.*

The proof of the result uses elementary arguments, and is omitted for the sake of brevity.

Once a value $k \geq k^\star$ has been fixed, the occurrence of k from the arguments of $A_2(\cdot)$ is removed to keep the notation streamlined, and to stress the fact that the selection of the gain k has already been made and $A_2(\mu,\varepsilon)$ is Hurwitz. The next proposition follows directly from [19, Lemma 2.1].

Proposition IV.2 *There exists $0 < \varepsilon^\star \leq 1$ such that for all $\varepsilon \in (0,\varepsilon^\star]$ there exists a solution $L(\mu,\varepsilon)$ of the quadratic matrix equation*

$$B_2(\mu) + A_2(\mu,\varepsilon)L(\mu,\varepsilon) - \varepsilon L(\mu,\varepsilon)\bar{F}^e(\mu) - \varepsilon L(\mu,\varepsilon)\bar{J}_{12}^e(\mu)C_2 L(\mu,\varepsilon)$$

which is approximated as

$$L(\mu,\varepsilon) = -A_2^{-1}(\mu,\varepsilon)B_2(\mu) - \varepsilon\, A_2^{-1}(\mu,\varepsilon)B_2(\mu)\big[\bar{F}^e(\mu) - \bar{J}_{12}^e(\mu)C_2 A_2^{-1}(\mu,\varepsilon)B_2(\mu)\big] + \mathcal{O}(\varepsilon^2).$$

Note that, since the matrix $B_2(\mu)$ appears in (34) scaled by ε, the change of coordinates required to bring (34) in the so-called "standard actuator form" is given by $\tilde{\chi}_2 = \chi_2 - \varepsilon L(\mu,\varepsilon)\tilde{z}^e$, where $\varepsilon \in (0,\varepsilon^\star]$. This transformation yields a singularly perturbed system in the form

$$\begin{aligned} \dot{\tilde{z}}^e &= \bar{F}^e(\mu,\varepsilon)\tilde{z}^e + \bar{J}_{12}^e(\mu)C_2\tilde{\chi}_2 \\ \varepsilon\dot{\tilde{\chi}}_2 &= \bar{A}_2(\mu,\varepsilon)\tilde{\chi}_2 \end{aligned} \qquad (35)$$

where

$$\bar{F}^e(\mu,\varepsilon) := \bar{F}^e(\mu) + \varepsilon\bar{J}_{12}^e(\mu)C_2 L(\mu,\varepsilon), \quad \bar{A}_2(\mu,\varepsilon) := A_2(\mu,\varepsilon) - \varepsilon^2 L(\mu,\varepsilon)\bar{J}_{12}^e(\mu)C_2,$$

from which it is now obvious to conclude the following result:

Proposition IV.3 *There exists $\varepsilon^{\star\star} \in (0,\varepsilon^\star]$ such that the system (35) is asymptotically stable for all $(\mu,\varepsilon) \in \mathcal{P} \times (0,\varepsilon^{\star\star}]$.*

The main result of the section is then summarized as follows:

Proposition IV.4 *Consider the dynamic error-feedback controller*

$$\begin{aligned} \dot{\xi}_2 &= \rho\Sigma_2\xi_2 + \Xi_2\xi_1 \\ u_2 &= \big[\lambda_1 + \Psi_2(\rho)\Xi_2 - \rho\,k\big]\xi_1 + \rho\Psi_2(\rho)[k\,I + \Sigma_2]\xi_2 - \rho\,k^2 e_2. \end{aligned} \qquad (36)$$

where λ_1 is the eigenvalue of the dynamic extension (22), $k > 0$ and $\rho > 0$ are tunable gain parameters, and (Σ,Ξ) and $\Psi(\rho)$ are given in (28) and (30), respectively. Choose $k > k^\star$ according to Proposition IV.1. Then, there exists $\rho^\star > 0$ such that for all $\rho \geq \rho^\star$ the controller (36) applied to system (25) achieves boundedness of all trajectories and asymptotic regulation of $e_2(t)$.

3. Outer-loop Controller

The theoretical development of the outer-loop controller follows along similar lines as the inner loop and will therefore be omitted for reasons of space, and only the final form of the controller will be given.

The reference model for the velocity reference is assumed to be the same as the one for the altitude reference (obviously, the set point will be different). Letting $\bar{S}_1$ be defined in the same way as $\bar{S}_2$, i.e. $\bar{S}_1 = \bar{S}_2$, an internal model for the steady-state control for the velocity dynamics is built as follows: Let (Σ_1, Ξ_1) be the pair in controller form

$$\Sigma_1 = \begin{pmatrix} 0 & 1 & 0 \\ 0 & 0 & 1 \\ -\sigma_3 & -\sigma_4 & -\sigma_5 \end{pmatrix}, \qquad \Xi_1 = \begin{pmatrix} 0 \\ 0 \\ 1 \end{pmatrix} \tag{37}$$

where the coefficients of the Hurwitz polynomial $p_{\Sigma_1}(s) = s^3 + \sigma_5 s^2 + \sigma_4 s + \sigma_3$ are chosen arbitrarily, in such a way that the roots of $p_{\Sigma_1}(s)$ are distinct from those of the polynomial $p_{S_1}(s)$. Let M_1 be the unique nonsingular solution of the Sylvester equation

$$M_1 \bar{S}_1 = \Sigma_1 M_1 + \Xi_1 Q_1 \tag{38}$$

and let $\Psi := Q_1 M_1^{-1}$. A candidate internal model for the steady-state input $u_1^*(t)$ is constructed as the dynamical system

$$\begin{aligned} \dot{\xi}_3 &= \Sigma_1 \xi_3 + \Xi_1 e_1 \\ v_1 &= \Psi_1 \xi_3 \end{aligned} \tag{39}$$

while the overall control input is chosen as

$$u_1 = -k_1 e_1 + \Psi_1 \xi_3 \tag{40}$$

where $k_1 > 0$ is large enough.

E. Controller implementation

The combined structure of the controller may now be written as

$$\begin{aligned} \dot{\xi}_0 &= \gamma \xi_0 + (\beta + \gamma) Q_f \\ \dot{\xi}_1 &= -\lambda \xi_1 + \delta_e \\ \dot{\xi}_2 &= \rho \Sigma_2 \xi_2 + \Xi_2 \xi_1 \\ \dot{\xi}_3 &= \Sigma_1 \xi_3 + \Xi_1 (V_t - r_1) \\ \delta_c &= -\kappa \xi_0 - \kappa Q_f \\ \delta_e &= \left[\lambda_1 + \Psi_2(\rho) \Xi_2 - \rho k \right] \xi_1 + \rho \Psi_2(\rho)[k\,I + \Sigma_2] \xi_2 - \rho k^2 (h - r_2) \\ \phi &= -k_1 (V_t - r_1) + \Psi_1 \xi_3 , \end{aligned} \tag{41}$$

whereas the procedure to tune the gains of (41) is summarized as follows:

- Choose the desired damping ratio and frequency (ζ, ω_n) for the reference model.

- Choose stable polynomials $p_{\Sigma_2}(s) = s^3 + \sigma_2 s^2 + \sigma_1 s + \sigma_0$ and $p_{\Sigma_1}(s) = s^3 + \sigma_5 s^2 + \sigma_4 s + \sigma_3$, in such a way that the roots of p_{Σ_2} are not too far from the $j\omega$-axis (recall that the roots will then be pushed to the left by increasing ρ), and such that they do not overlap with the roots of $p_{\bar{S}_2}(s)$.

- Choose the position of the rate gyro sensor and the auxiliary controller parameters γ, β and κ such that the original zero dynamics (18) are stabilized for a given range of fuel conditions and flight conditions.

- Choose $\lambda > 0$.

- Fix $\rho = 1$, and compute (the smallest) $k^\star$ such that the matrix $A_2(\mu, 1, k)$ is Hurwitz for all μ considered (that is, for all possible perturbed models). Fix a value $k \geq k^\star$.

- Increase ρ until the system (34) is asymptotically stable for all perturbed models.

- Choose k_1 such that the overall closed-loop system is asymptotically stable.

American Institute of Aeronautics and Astronautics

V.   Simulation Results for the Robust Output Feedback Design

The performance of the robust output feedback control design is evaluated on the nonlinear model (1). The references are filtered steps with respect to the trim condition of 1000 ft/s and 10000 ft for the vehicle velocity and altitude, respectively. Since the airbreathing-hypersonic vehicle is not intended for highly aggressive maneuvers, we shall allow ourselves to use a reference that settles in about 140sec (1% settling). Note that in previous works[4–7] a faster reference was used, settling after around 100 sec, but in those cases the non-linear model did not encompass heave coupling with the flexible dynamics, and perfect full state measurement was assumed. The gains for the robust controller, shown in Table 5, were tuned and validated by verifying that they stabilized the closed loop system using a given family of linearized models of the nonlinear plant. Linearizations have been performed using 5 trim conditions and two fuel conditions, namely 90% and 50% fuel load. Figures 13-14 show the results of closed-loop simulation for a 90% fuel condition while Figures 15-16 show the same for a 50% fuel condition. It is evident from Figures 13(c)-13(b) and 15(c)-15(b) that the tracking performance is near perfect and Q_f is well regulated for both fuel conditions. Furthermore, Figures 13(a) and 15(a) show that the inputs are fairly well behaved for both fuel conditions, as they are within their saturation limits of $[0,1]$ for ϕ, and ± 0.52rad for δ_e and δ_c. Here, some differences between the responses for the two fuel conditions can be observed, as a smaller ϕ is needed to maintain the target speed at the 50% fuel condition. When the filtered step reference is applied, a noticeable oscillating transient due to the coupling with the flexible dynamics can be observed; this behavior stems from the use of a fairly high-gain feedback, and may be mitigated by a more careful judicious choice of the controller gains. The angle of attack deviates only slightly from trim and is quite well behaved for both fuel conditions as can be seen from Figures 14(a) and 16(a). Figures 14(b) and 16(b) show that the flight path angle is kept reasonably small and smooth for both fuel conditions. Finally, Figures 14(c), 16(c), 14(d), and 16(d) show that the flexible states and controller states are stable and settle to constant values. The controller dynamics were implemented in a balanced realization to avoid numerical problems with the control canonical form. Thus the states shown in Figures 14(d) and 16(d) do not relate directly to the controller dynamics states given in previous sections but through a linear transformation not given here for reasons of space.

VI.   Conclusion

In this study, we found that linear observer-based output feedback can be successfully applied to a nonlinear air-breathing hypersonic vehicle model for a very limited range of operating conditions. Modeling of rate and acceleration sensors which include flexible effects provided insight into the effect of sensor placement, which led to the development of a performance index focused on improving system observability. The locations of high observability, near the nose and tail of the aircraft, agree with previous work in sensor placement for flight vehicles. Since the observer is constructed with linearized equations of motion, the observer is only valid for an operating range around the trim condition, and offers poor robustness with respect to parameter variations. This limitation, inevitable with a linear observer, has been overcome by designing a robust dynamic output-feedback controller which does not rely on asymptotic state reconstruction. Despite the fact that the robust controller constitutes a significant improvement over the observer-based design, there is still room for improvement. The fact that part of the controller is designed using high-gain feedback, forces the reference trajectories to be rather slow, to avoid inducing considerable oscillations in the inputs during the transient. A more sophisticated design based on adaptive control or gain-scheduling may alleviate the need for such high-gain feedback, and yield improved tracking capabilities.

Table 5. Controller Parameters & Sensor Placement

Rate Gyro Placement (from front)	Aux. Controller		Other Controller Param.	
26 ft	κ	10	λ	1
	β	5	k	138.6
	γ	1	ρ	1
			k_1	1

American Institute of Aeronautics and Astronautics

(a) Inputs to the plant

(b) Measured Pitch Rate

(c) Output: Velocity & Reference

(d) Output: Altitude & Reference
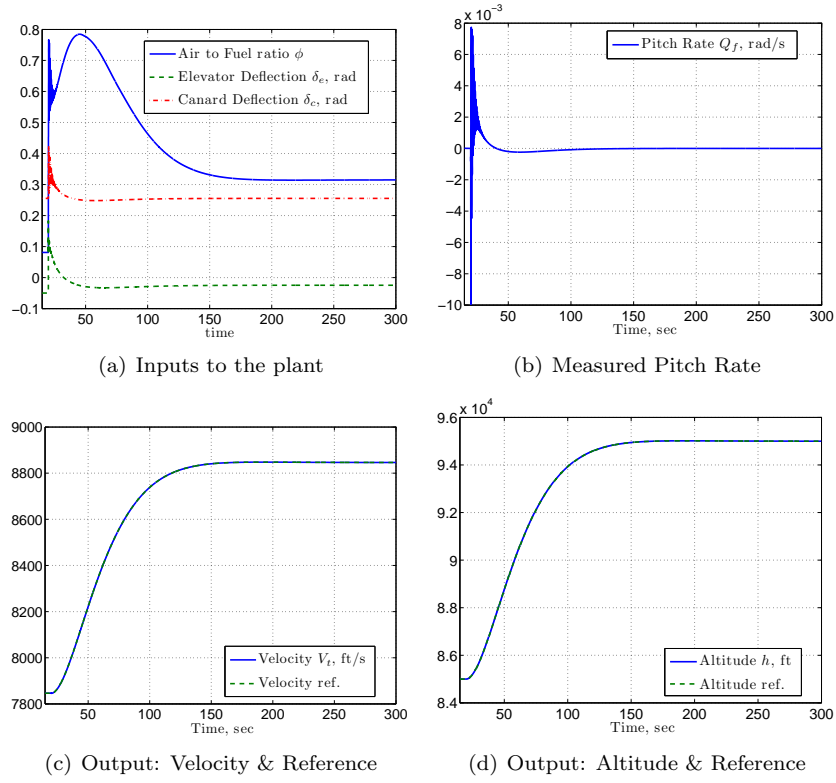
Figure 13. Plant inputs and outputs using a 90% fuel condition

(a) Angle of Attack

(b) Flight Path Angle

(c) Flexible States

(d) States of the Balanced Controller
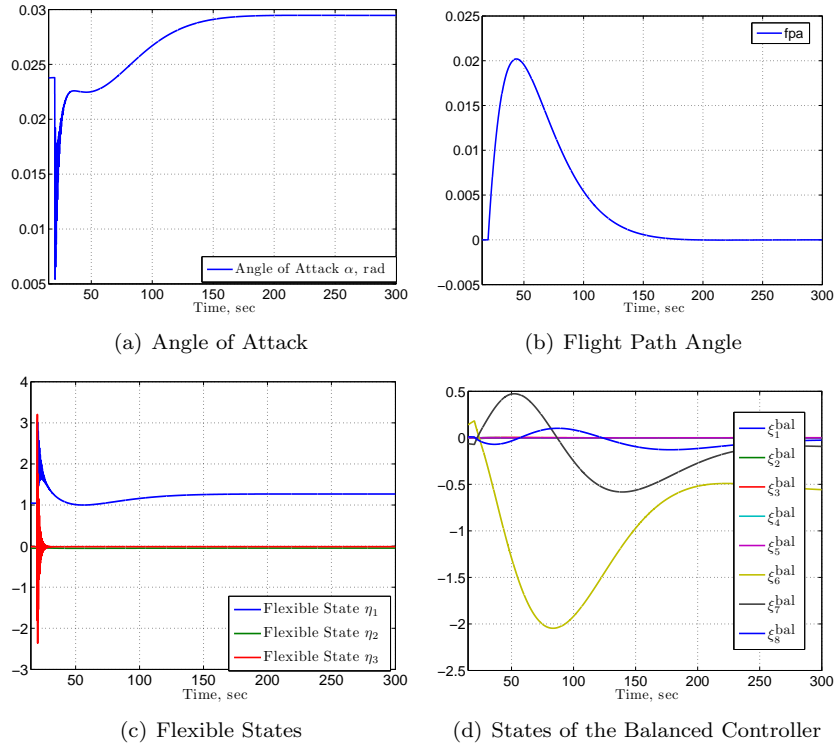
Figure 14. Angle of attack, FPA, flexible states, and state of the controller for a 90% fuel condition

(a) Inputs to the plant

(b) Measured Pitch Rate

(c) Output: Velocity & Reference

(d) Output: Altitude & Reference
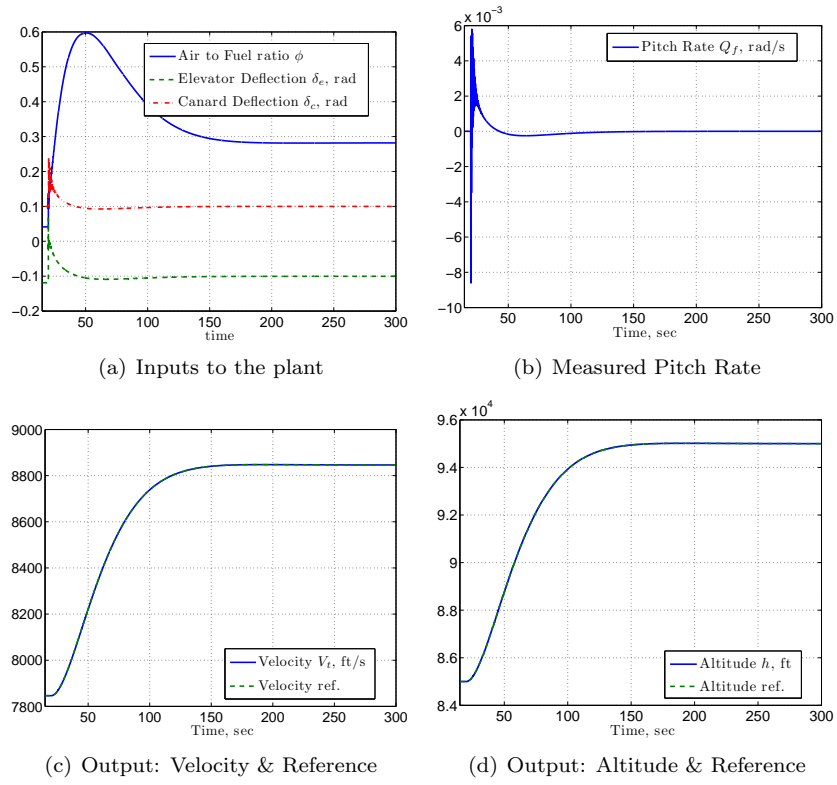
Figure 15. Plant inputs and outputs using a 50% fuel condition

(a) Angle of Attack

(b) Flight Path Angle

(c) Flexible States

(d) State of the Balanced Controller
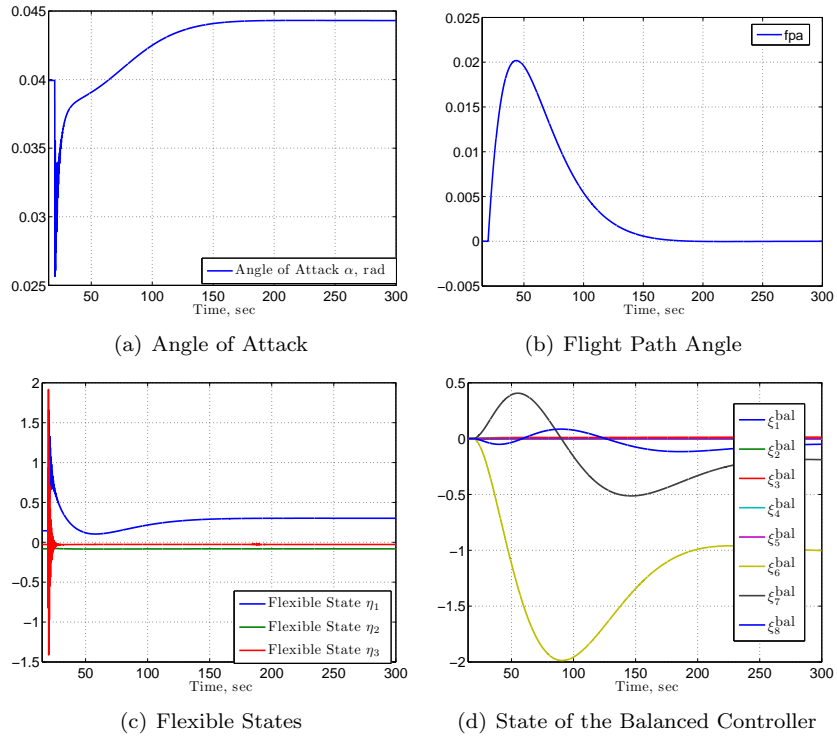
Figure 16. Angle of attack, FPA, flexible states, and state of the dynamic controller for a 50% fuel condition

American Institute of Aeronautics and Astronautics

Acknowledgments

References

[1] Bolender, M. A. and Doman, D. B., "A Nonlinear Longitudinal Dynamical Model of an Air-breathing Hypersonic Vehicle," *Submitted to AIAA Journal of Spacecraft and Rockets*, 2006.

[2] Bilimoria, K. D. and Schmidt, D. K., "Integrated Development of the Equations of Motion for Elastic Hypersonic Flight Vehicles," *Journal of Guidance, Control, and Dynamics*, Vol. 18, No. 1, 1995, pp. 73–81.

[3] Xu, H., Mirmirani, M., and Ioannou, P., "Adaptive sliding mode control design for a hypersonic flight vehicle," *AIAA Journal of Guidance, Control, and Dynamics*, Vol. 27, No. 5, 2004, pp. 829–38.

[4] Parker, J. T., Serrani, A., Yurkovich, S., Bolender, M. A., and Doman, D. B., "Approximate Feedback Linearization of an Air-breathing Hypersonic Vehicle," *Proceedings of AIAA Guidance, Navigation, and Control Confrence*, 2006.

[5] Groves, K. P., Sigthorsson, D. O., Serrani, A., Yurkovich, S., Bolender, M. A., and Doman, D. B., "Reference Command Tracking for a Linearized Model of an Air-breathing Hypersonic Vehicle," *AIAA Guidance, Navigation, and Control Conference*, 2005.

[6] Sigthorsson, D. O., Serrani, A., Yurkovich, S., Bolender, M. A., and Doman, D. B., "Tracking Control For An Overactuated Hypersonic Air-Breathing Vehicle With Steady State Constraints," *AIAA Guidance, Navigation, and Control Conference*, 2005.

[7] Sigthorsson, D. O. and A. Serrani, A., "Tracking with Steady-State Optimization: an Application to Air-Breathing Hypersonic Vehicle Control," *IEEE 14th Mediterranean Conference on Control and Automation*, 2006.

[8] Schmidt, D. K. and Velapoldi, J. R., "Flight Dynamics and Feedback Guidance Issues for Hypersonic Air-breathing Vehicles," *Proceedings of AIAA Guidance, Navigation, and Control Conference and Exhibit*, No. AIAA-1999-4122, Portland, OR, 1999, pp. 859–871.

[9] Schmidt, D. K., "Optimum mission performance and multivariable flight guidance for air-breathing launch vehicles," *Journal of Guidance, Control, and Dynamics*, Vol. 20, No. 6, 1997, pp. 1157–64, Nonlinear Dynamical Systems.

[10] Tournes, C., Landrum, D. B., Shtessel, Y., and Hawk, C. W., "Ramjet-powered reusable launch vehicle control by sliding modes," *Journal of Guidance, Control, and Dynamics*, Vol. 21, No. 3, 1998, pp. 409–15.

[11] Doman, D. B. and Ngo, A. D., "Dynamic inversion-based adaptive/reconfigurable control of the X-33 on ascent," *Journal of Guidance, Control, and Dynamics*, Vol. 25, No. 2, 2002, pp. 275–84.

[12] Van der Velde, W. and Carignan, C., "Number and Placement of Control System Components Considering Possible Failures," *AIAA Journal of Guidance, Control, and Dynamics*, Vol. 7, 1984, pp. 703–709.

[13] Al-Shehabi, A. and Newman, B., "Optimal blending filter parameters and sensor placement for flight control," *AIAA Guidance, Navigation, and Control Conference and Exhibit, Monterey, CA*, 2002.

[14] Williams, T., Bolender, M. A., Doman, D. B., and Morataya, O., "An Aerothermal Flexible Mode Analysis of a Hypersonic Vehicle," AIAA Paper 2006-6647, Aug. 2006.

[15] Bolender, M. A. and Doman, D. B., "Flight Path Angle Dynamics of Air-breathing Hypersonic Vehicles," *Proceedings of AIAA Guidance, Navigation, and Control Confrence*, 2006.

[16] Meirovitch, L., *Analytical Methods in Vibration*, McMillan Publishing Co., New York, 1967.

[17] Stevens, B. L. and Lewis, F. L., *Aircraft Control and Simulation*, John Wiley and Sons, Inc., 2nd ed., 2003.

[18] Bay, J. S., *Fundamental of Linear State Space Systems*, McGraw-Hill, 1999.

[19] Kokotovic, P., O'Reilly, J., and Khalil, H., *Singular Perturbation Methods in Control: Analysis and Design*, Academic Press, Orlando, FL, 1986.